

PAPER

The role of topology in microstructure-property relations: a 2D DEM based study

To cite this article: Katerine Saleme Ruiz and Maria Emelianenko 2018 *Modelling Simul. Mater. Sci. Eng.* **26** 014001

View the [article online](#) for updates and enhancements.

Related content

- [Stochastics of Diffusion Induced Damage in Intercalation Materials](#)
Pallab Barai and Partha P Mukherjee
- [Investigation of primary static recrystallization in a NiTiFe shape memory alloy subjected to cold channelling compression using the coupling crystal plasticity finite element method with cellular automaton](#)
Yanqiu Zhang, Shuyong Jiang, Li Hu et al.
- [Spatial clustering strategies for hierarchical multi-scale modelling of metal plasticity](#)
M Khairullah, J Gawad, D Roose et al.

The role of topology in microstructure-property relations: a 2D DEM based study

Katerine Saleme Ruiz ¹ and Maria Emelianenko 

Department of Mathematical Sciences, George Mason University, Fairfax, VA 22030, United States of America

E-mail: katerinesaleme@gmail.com

Received 23 May 2017, revised 18 October 2017

Accepted for publication 30 October 2017

Published 4 December 2017



CrossMark

Abstract

We compare Rényi entropy-based mesoscale approaches for characterizing 2D polycrystalline network topology and geometry, based on the grain number of sides and grain areas, respectively. We study the effect of microstructure disorder on mechanical properties such as elastic and damage response by performing simulations of quasi-static uniaxial compression loading tests on an idealized material using grain-level micro-mechanical discrete element model. While not comprehensive enough to make general conclusions, this study allows us to make observations about the sensitivity of mechanical parameters such as Young's modulus, proportional limit, first yield stress, toughness and amount of microstructure damage to different entropy measures.

Keywords: topology, entropy, polycrystalline materials, microstructure, discrete element method

(Some figures may appear in colour only in the online journal)

1. Introduction

Development of approaches to quantify polycrystalline grain morphology and understand its role in the microstructure-property relations is of critical importance for many materials applications. Materials simulation software (e.g. phase field, Potts model, vertex models etc), especially those relying on the finite element method, often use Voronoi tessellations as a way of representing the grain boundary network in a polycrystalline microstructure [1–7]. A review of the Voronoi tessellation approach and properties can be found in [8]. Alternatives based on physically-driven simulations of annealing or recrystallization [9–11], or algorithms that attempt to directly reproduce statistical data coming from experimental characterizations

¹ Author to whom any correspondence should be addressed.

[12] have been introduced, which are more accurate in representing realistic microstructures, but often come with additional computational challenges [13].

Despite its popularity and obvious advantages due to its relation with unstructured meshing techniques, the Voronoi approach is inherently phenomenological and can potentially introduce a bias related to the suboptimal choice of the microstructure type. Indeed, the effect of the distribution of Voronoi cell generators on microstructure and materials properties is not fully understood [14]. Going beyond the work performed by Silva *et al*, we carry out sensitivity analysis to investigate dependence between materials mechanical response and mesoscale representations of a microstructure network by perturbing Voronoi generators in several different ways. The fundamental idea in this study is to find appropriate measure(s) of morphology that would be sensitive enough to capture variations in mechanical behavior.

One way to characterize morphological features is based on the concept of entropy. The first definition of entropy (developed by Rudolf Clausius in the 1850s) came from the field of thermodynamics. In [15], Berdichevsky introduced the notion of microstructure entropy as a key thermodynamical parameter in a micro-plasticity model, and later described how to select (from the experiments) the probabilistic measure used to compute the entropy of random structures using the analysis of the homogenization problem [16]. An alternative definition of entropy (developed by Ludwig Boltzmann in the 1870s) came from statistical mechanics field. This definition leads to the interpretation of entropy as a measure of *disorder*. One of the first attempts to apply entropic measure of this type to quantify the topology of the grain boundary network is due to Mason *et al* [1]. In our study we quantify the statistical topology and geometry of the grain boundary network using the Rényi entropy approach motivated by the work of A-iyeh and Peters aimed at measuring information levels of Voronoi tessellations in the context of image analysis [8]. In the special case of grain size-based Shannon entropy this measure coincides with the relative density measure considered in [14]. Following [1], we use the concept of Jensen–Rényi divergence to measure *distances* between grain boundary networks.

The main objective of this work is to use Rényi entropy measures to analyze the sensitivity of the mechanical response to the microstructure topology and geometry and find measure(s) suitable for a given purpose. One may employ a variety of modeling methodologies when it comes to simulating elasto-plastic response of polycrystals. We chose the discrete element method (DEM) as a tool for analyzing mechanical response for a given microstructure. This choice is in part motivated by the fact that DEM allows to capture both intergranular and transgranular microcrack initiation and evolution in polycrystalline materials, in addition to standard elastic regime. In our code we use linear grain-level micromechanical model based on DEM using bonded contacts, prismatic particles and improved fracture criteria. Conclusions of this work are limited to DEM-based algorithms and as such should not be extrapolated to other simulation methodologies. Alternative candidates include phase field models [17], Monte Carlo Potts algorithms [18], cellular automata [19] and level set methods [20, 21], which are used in a variety of engineering software products. While comparative study between models is outside the scope of this work, the authors feel that this investigation should prompt future research in this area. Since this study is primarily concerned with the topological and geometrical information related to grain numbers of sides and grain areas, respectively, we are only considering the case of crystallographic isotropy and do not include grain growth and recrystallization processes. Other parameters such as misorientations and dihedral angles can be explored under the same framework and will be the subject of future investigations.

The paper is organized as follows: in section 2 the procedure for generating the polycrystalline microstructures is presented. Then a measure of microstructure geometrical and topological and geometrical disorder based on the Rényi entropy is introduced together with the description of the DEM model used to perform simulations of uniaxial compression tests

on the microstructures. In section 3 numerical results are presented. Stress–strain curves produced by DEM simulation are followed by scatter plots of the mechanical response with respect to the different entropy measures. The effects of mesoscale topological parameters on the mechanical behavior of polycrystalline materials are analyzed. Finally, in section 4 several concluding remarks are presented.

2. Methods

2.1. Microstructure generation

Two types of 2D microstructures on a rectangular specimen with a height to width ratio of 2 are considered in this study:

- (i) The hexagonal structure consisting of hexagonal cells. It is a Voronoi tessellation of a hexagonal lattice.
- (ii) The perturbed structure. It is generated by taking a Voronoi tessellation of a perturbed hexagonal lattice in which the centers of Voronoi cells are displaced in a random direction by a distance sampled from four different distributions:
 - (a) Normal distribution with a standard deviation and mean of $\frac{1}{5}$ and $\frac{1}{20}$ of the lattice spacing respectively.
 - (b) Weibull distribution with scale parameter and shape parameter of $\frac{1}{5}$ and $\frac{1}{2}$ of the lattice spacing respectively.
 - (c) Poisson distribution with parameter λ equals the lattice spacing.
 - (d) Lognormal distribution with a standard deviation and mean of $\frac{1}{5}$ and $\frac{1}{20}$ of the lattice spacing respectively.

Perturbed microstructures of type (a)–(d) are called Normal-Voronoi, Weibull-Voronoi, Poisson-Voronoi and Lognormal-Voronoi respectively. The parameters in the Normal and Poisson distributions above are taken to be the same as in [1]. The rest of the perturbations have not been studied in this context before. A variety of topologies can be observed in figure 1 with shows representative samples of the hexagonal and perturbed reference microstructures.

2.2. Microstructure entropy

The topology and geometry of a 2D microstructure X representing a polycrystalline material consisting of a total of N grains can be described by a probability distribution $p(A)$ of a certain discrete or continuous random variable A that can represent any relevant network parameter. In discretized form, it is convenient to represent $p(A)$ as a vector $p^k(A)$, where index $k = 1, \dots, K$ denotes a certain equivalence class (a certain bin in the corresponding histogram). In this work we consider two types of random variables:

Type 1. Grain size. In this case, the continuous random variable A represents grain sizes, or areas in two-dimensional setting. Hence $p^k = \mathbb{P}(A = A_k)$ is the probability of observing a grain in k th class based on its size. If A_T is the total planar surface area of a Voronoi tessellation X representing certain material, then

$$p^k = \frac{A_k}{A_T}, \quad \sum_{k=1}^K p^k = 1. \quad (1)$$

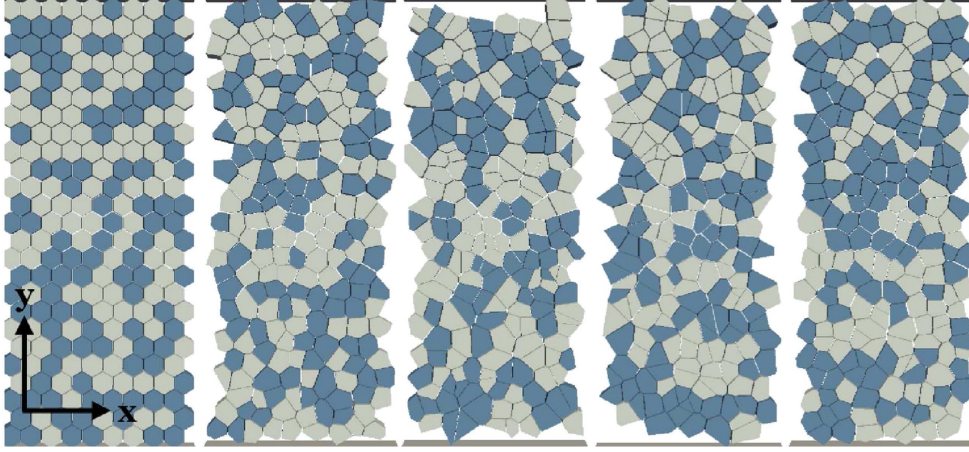


Figure 1. From left to right, representative samples of the hexagonal, Normal-Voronoi, Weibull-Voronoi, Poisson-Voronoi and Lognormal-Voronoi reference microstructures.

Type 2. Number of sides. This is an example of a discrete random variable, where A_i represents the number of sides of i th grain. Here $p^k = \mathbb{P}\{A = k\}$ is the probability that a given grain has exactly k sides. Let $I(k)$ be the number of k -sided polygons in the microstructure X . Then

$$p^k = \frac{I(k)}{N}, \quad \sum_{k=1}^K p^k = 1. \quad (2)$$

Several statistical measures can be used to characterize microstructures based on these distributions. In this study we are focusing on the Rényi entropy which generalizes the notion of Shannon entropy used in prior work of Mason *et al* [1].

The Rényi entropy [22] provides the information of order $\beta \geq 1$ of the quality of the random microstructure X generated via Voronoi tessellation and is calculated as

$$\eta_\beta(X) = \frac{1}{1 - \beta} \ln \sum_{k=1}^K (p^k)^\beta, \quad \beta = 1.5, 2.0, 2.5. \quad (3)$$

The standard Shannon entropy represents a limiting case of $\beta = 1$:

$$\eta_S(X) = -\sum_{k=1}^K p^k \ln(p^k) = \lim_{\beta \rightarrow 1} \eta_\beta(X). \quad (4)$$

Both of these quantities are used to measure the disorder of a graph-like structure (in this case, grain boundary network).

2.3. Distance between microstructures

To quantify the topological and geometrical differences between two microstructures X and Y we use the metric defined as a square root of the Jensen–Rényi divergence with equal weights:

$$\text{Dist}_{\text{JR}_\beta} = \sqrt{\eta_\beta(p_Z) - \frac{1}{2}\eta_\beta(p_X) - \frac{1}{2}\eta_\beta(p_Y)}, \quad (5)$$

where $p_Z = \frac{1}{2}p_X + \frac{1}{2}p_Y$ and p_X and p_Y are the probability distributions for X and Y respectively. For the limiting case when $\beta \rightarrow 1$, we use the metric defined as the square root of the Jensen–Shannon divergence with equal weights:

$$\text{Dist}_{\text{JS}} = \sqrt{\eta_S(p_Z) - \frac{1}{2}\eta_S(p_X) - \frac{1}{2}\eta_S(p_Y)}. \quad (6)$$

2.4. DEM model

To simulate the mechanical behavior of 2D polycrystalline materials with microstructures generated as described in section 2.1, we used the non-spherical discrete element modeling code (ERDC-DEM) originally described by [23, 24] to model intergranular microcrack initiation and evolution by adopting a simplified description of the bonded particle model proposed by [25]. DEM simulations of the interaction between rigid particles is based on the numerical solution of Newton's second law of motion using the velocity Verlet algorithm.

The contact forces are computed and then integrated to determine particle motions. The normal (\vec{F}_n^s) and shear (\vec{F}_t) components of the contact force are calculated from a modified Hooke's model with parallel viscous damping and a Coulomb friction cap on the tangential force as described below:

$$\vec{F}_n^s = -K_n \vec{U}_n,$$

$$\vec{F}_t = \begin{cases} -(K_s \vec{U}_s), & \|\vec{F}_t^s\| < \|\vec{F}_n^s\| \mu_s, \\ \vec{F}_t^s \left(\frac{\vec{F}_{fs}}{\|\vec{F}_t^s\|} \right), & \|\vec{F}_t^s\| \geq \|\vec{F}_n^s\| \mu_s, \|\vec{F}_t^s\| \neq 0, \end{cases}$$

where U_n is the projection vector of relative displacement, \vec{U}_r , on normal vector, \vec{n} , between the particles centers. $U_s = U_r - U_n \vec{n}$ is the projection vector of the relative displacement on shear vector, \vec{s} ; and μ_s is the sliding friction coefficient. The relative displacement \vec{U}_r is computed in terms of the translational (V) and rotational (V_t) velocities of particles A and B as:

$$\vec{U}_r = \Delta t((V_B + V_{tB}) - (V_A + V_{tA})).$$

And the Coulomb frictional forces are computed as:

$$\vec{F}_{fr} = \vec{F}_{ft} = -\vec{F}_n \mu_r, \quad \vec{F}_{fs} = -\vec{F}_n \mu_s,$$

where μ_r is the rolling coefficient of friction and μ_s is the sliding coefficient of friction.

The contact is a Kelvin model, represented by a purely viscous damper and a purely mechanical spring connected in parallel. The Coulomb contact and the bonding are assumed to act in parallel, so that the behavior of a collection of grains joined by bonded contacts can be simulated. The normal (F_{bn}) and the shear (F_{bs}) forces due to bonding are computed as:

$$F_{bn} = K_{bn} \Delta v_n \Delta t, \quad F_{bs} = K_{bs} \Delta v_s \Delta t,$$

where K_{br} is the spring rotational stiffness and K_{bt} is the spring torsional stiffness. Failure occurs when the total force and total moment due to any of the contact modes exceeds the limits for a combined yield criterion. Bond failure due to tension, shear bending and torsion occurs when the corresponding bonding force exceeds the particle-to-particle corresponding strength. The normal, shear, rolling and torsional limits of failure are computed respectively

as:

$$\begin{aligned} F_{bn_limit} &= t_{bn}A_b, & F_{bs_limit} &= t_{bs}A_b, \\ M_{r_limit} &= t_{bn}\left(\frac{I}{r}\right), & M_{t_limit} &= t_{bs}\left(\frac{J}{r}\right), \end{aligned}$$

where t_{bn} is the bond normal strength and t_{bs} is the bond shear strength. $I_b = 0.25\pi r^4$ is the area moment of inertia and $J_b = 2I_b$ is the polar moment of inertia.

Following classical theory (see e.g. [26, 27] and references therein), equivalent Cauchy stress tensor is computed for each discrete element as

$$\bar{\sigma}_i = \frac{1}{2V_i} \left[\frac{1}{2} \sum_j \vec{d}_{ij} \otimes \vec{F}_{ij} + \vec{F}_{ij} \otimes \vec{d}_{ij} \right], \quad (7)$$

where \otimes is the tensor product, $\bar{\sigma}_i$ is the equivalent Cauchy stress tensor of the discrete element i , V_i is the volume of the discrete element i , \vec{F}_{ij} is the total contact force exerted on the discrete element i by the discrete element j and \vec{d}_{ij} is the moment arm vector between the centroid of the discrete element i and each contact point with the discrete element j . The formulation in equation (7) ensures that the computed particle stress tensor ($\bar{\sigma}_i$) is symmetric and it has been used to compute an approximated stress tensor ($\bar{\sigma}$) in discrete systems with N_p particles [28–30]:

$$\bar{\sigma} = \frac{1}{V} \left[\sum_i^{N_p} V_i \bar{\sigma}_i \right]. \quad (8)$$

Since DEM tracks each individual particle's motion, to accurately mimic materials' behavior DEM requires calibration of the particle-level parameters (such as particle density, modulus of elasticity, and coefficient of friction). For coarse materials these parameters are relatively easy to measure and the ERDC-DEM modeling code used in this study has been validated for granular materials as reported in [23]. However for cohesive materials composed of fine particles obtaining direct measurements of particle-level parameters is nearly impossible, since most of the phenomena occurring at the micro-scale cannot even be directly observed. For cohesive materials, parameter calibration mainly consists on replicating bench-scale physical experiments with DEM simulations and then modify the particle's parameters to optimize the results. The parameters used in our simulations are the result of this type of calibration.

3. Numerical results

3.1. Setup

Our benchmarking set includes the hexagonal lattice as well as 4 sets of microstructures each consisting of 25 samples on a rectangular domain $D = [0, 100] \times [0, 200]$ mm². As described in section 2.1, each set corresponds to one of the following types: (a) Normal-Voronoi perturbation; (b) Weibull-Voronoi perturbation; (c) Poisson-Voronoi perturbation; (d) Lognormal-Voronoi perturbation.

For each microstructure, discrete area probabilities p^k were calculated using equation (1) and considering $K = 24$ equivalence classes (bins); each class representing the grain areas in the ranges $[A_k, A_{k+1}]$, where $A_k = 5n$ and $n = 3, 4, \dots, 26$, which covers the range of the values we have observed in the sampled data. Similarly, discrete side probabilities were

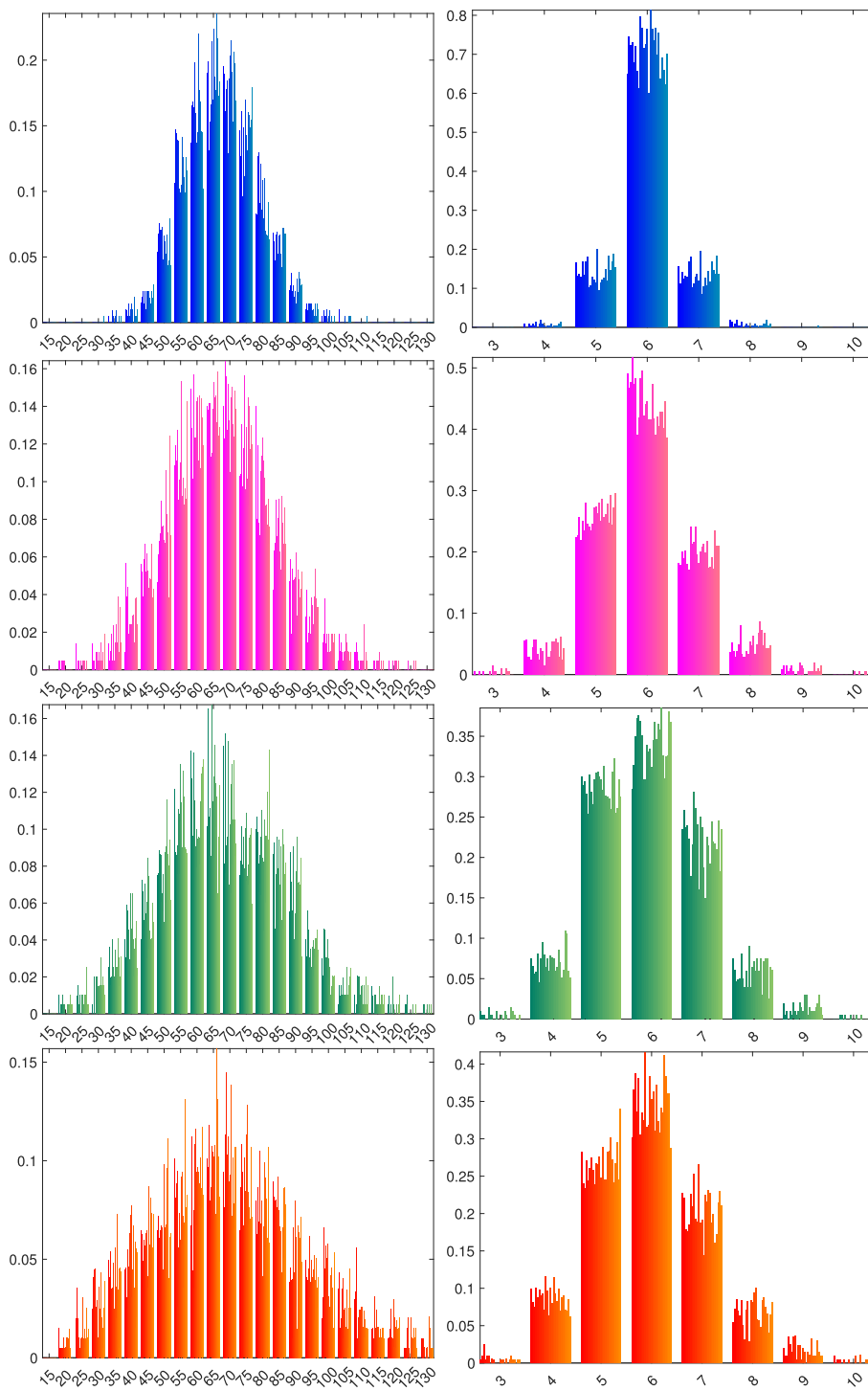


Figure 2. Histograms of: (left) size distribution and (right) number of sides distribution. From top to bottom: Normal-, Weibull-, Poisson- and Lognormal-Voronoi microstructures.



Figure 3. Schematic view of microstructure ordering based on entropy calculations. Hexagonal microstructure has the minimum entropy value equal to zero.

Table 1. DEM contact parameters used for the simulation tests.

Input parameters	Values	Units
Time step increment	0.00001	s
Particle size	varies	mm
Particle specific gravity	3.10	kg/10 ⁹ mm ³
Gap for initial contact	0.03	mm
Particle–particle normal spring stiffness constant	1000	N mm ⁻¹
Particle–particle shear spring stiffness constant	100	N mm ⁻¹
Particle–particle rolling stiffness constant	0.0	N mm rad ⁻¹
Particle–particle torsional stiffness constant	0.0	N mm rad ⁻¹
Particle–particle inverse of coefficient of restitution	10.0	—
Particle–particle Coulomb sliding friction coefficient	0.5	—
Particle–particle Coulomb rolling friction coefficient	0.5	—
Particle–wall normal spring stiffness constant	10000	N mm ⁻¹
Particle–wall shear spring stiffness constant	1000	N mm ⁻¹
Particle–wall rolling stiffness constant	0.0	N mm rad ⁻¹
Particle–wall torsional stiffness constant	0.0	N mm rad ⁻¹
Particle–wall inverse of coefficient of restitution	10.0	—
Particle–wall Coulomb sliding friction coefficient	0.0	—
Particle–wall Coulomb rolling friction coefficient	0.0	—

calculated using equation (2) considering $K = 8$ classes; each one representing the number of grain sides varying from 3 to 10. Histograms of the areas and number of sides probability distributions for each of the four microstructure sets are shown in figure 2.

Both sets of probabilities were used to compute entropy values using equations (3) and (4). Specifically, Shannon entropy and Rényi entropy with $\beta = 1.5, 2.0, 2.5$ values were calculated for the four sets of the referenced microstructures. These entropy values are a measure of the degree of disorder in the microstructure: the higher the entropy value the larger the degree of the disorder in the microstructure. It is worth noting all size and side based entropy calculations order the four microstructure sets as illustrated in figure 3; with the exception of few Lognormal microstructures which have entropy values overlapping with entropy ranges for Weibull and Poisson microstructure sets. From the entropy calculations and the distribution histograms we observed that as the tails of the size and side histograms get fatter, the entropy values increase. Normal-Voronoi microstructures have the thinner histogram tails and smaller entropy values, followed by Weibull-Voronoi, and then by Poisson-Voronoi microstructures. Lognormal-Voronoi microstructures have the fatter histogram tails and the higher entropy values with few exceptions.

On each of these 101 samples, we performed DEM simulations of quasi-static uniaxial compression loading for rectangular solids with contact parameters described in table 1 and bonded parameters described in table 2. Loading was applied in the y -direction and the top and bottom wall moved inwards with a velocity of 0.2 mm s^{-1} . Simulations were run for up to 50000 time steps and the critical time step required to ensure that the numerical scheme will

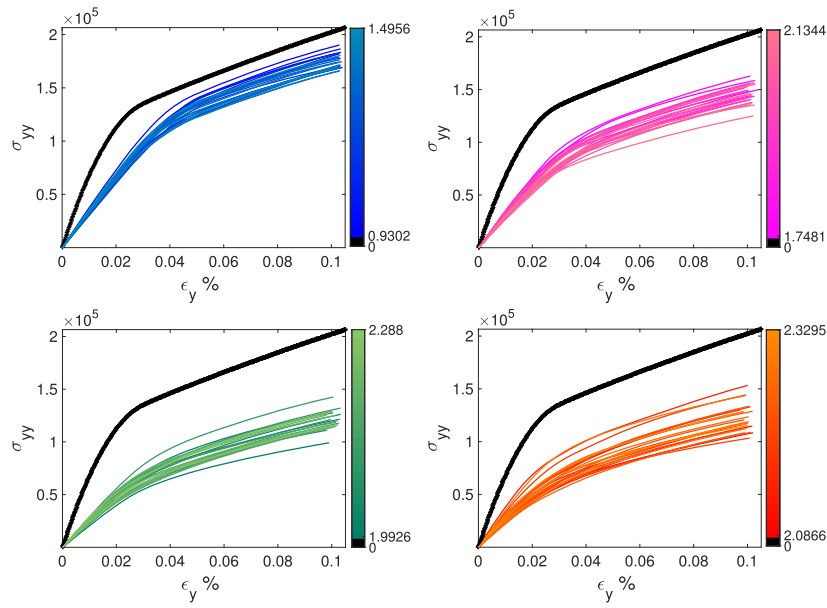


Figure 4. Stress–strain curves for: (top left) Normal-Voronoi, (top right) Weibull-Voronoi, (bottom left) Poisson-Voronoi, and (bottom right) Lognormal-Voronoi microstructures compared against the stress–strain curve for the hexagonal microstructure (thicker curve).

Table 2. DEM bonding parameters used in the drop and uniaxial compression simulation tests.

Bonding input parameters	Values	Units
Bond normal stiffness	500	N mm ⁻³
Bond shear stiffness	100	N mm ⁻³
Bond normal ‘compressive’ strength	1000	N mm ⁻²
Bond shear strength	1000	N mm ⁻²

remain stable during the simulation was approximated as $t_{\text{critical}} = 2\sqrt{\frac{m}{k}}$, where m is the mass of the smallest particle and k is the constant spring stiffness of the smallest particle.

3.2. Mechanical response

From the DEM calculations, the longitudinal strain percentage was calculated by averaging the vertical length decrease, the stress values for each grain were calculated using equation (7) and the corresponding normal stress for the specimen in the y -direction ($\bar{\sigma}_{yy}$) was calculated using equation (8). The specimen stress calculation was limited only to the middle one-third of the specimen to avoid boundary effects. Resulting stress–strain curves are shown in figure 4, where the perfectly hexagonal microstructure response corresponds to the thicker curve, which has the minimum entropy value $\eta = 0$ representing zero disorder. Solid curves correspond to (top left) Normal-Voronoi microstructures, (top right) Weibull-Voronoi microstructures, (bottom left) Poisson-Voronoi microstructures, (bottom right) Lognormal-Voronoi microstructures.

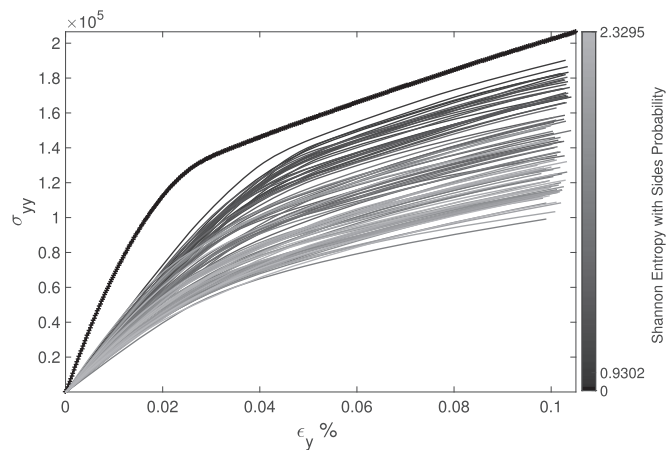


Figure 5. Stress–strain curve with gray scale based on Shannon side-based entropy values. Thicker curve corresponds to the hexagonal microstructure.

Table 3. Mechanical parameters for hexagonal microstructure.

Mechanical parameter	Value	Units
Young's modulus	677	MPa
Proportional limit	86	kPa
First yield stress	90	kPa
Toughness	155	Pa × %

All stress–strain curves were plotted together in figure 5. Curves were colored using gray scale based on side-based Shannon entropy values, the darker the curve the smaller the entropy value. The stress–strain curves for Normal-Voronoi microstructures are closer to the hexagonal curve than the rest of the microstructures. From these stress–strain curves, several mechanical parameters were extracted: Young's modulus, proportional limit, first yield stress and toughness. The elastic modulus is determined from the Hook's law as the ratio of stress to strain ($E = \sigma/\epsilon$). Specifically it is determined as the slope of the tangent to the stress–strain curve at a point in which the ratio of change in stress to change in strain is maximum. The first yield is the stress beyond which the material is no longer elastic and the toughness is the area under the stress–strain curve. Elastic parameters for the hexagonal microstructure are presented in table 3. The mechanical parameters were plotted against their corresponding *entropy* values: Young's modulus in figure 6, proportional limit in figure 7, first yield stress in figure 8 and toughness in figure 9. In all the scatter plots circles, diamonds, squares and triangles correspond to parameter values of Normal-, Weibull-, Poisson- and Lognormal- Voronoi microstructures respectively. From these scatter plots we observed that, all of the elastic parameters have a nonlinear trend with respect to the four entropies based on both size and side statistics. Overall, the larger the entropy value the weaker the mechanical performance of the material. However, in the scatter plots for the size based entropy, few Lognormal-Voronoi microstructures with the largest entropies values surprisingly do not have the smallest values for the elastic parameter as expected. On the contrary, the scatter plots for the side based entropy clearly shows a strictly non linear decreasing trend, with the exception of Young's modulus which behaves similar to the size based plots.

Also, entropy data naturally cluster in terms of microstructure type. In fact, the closer the Rényi parameter β is to 1, the more distinguished the clusters are, especially in the plots for

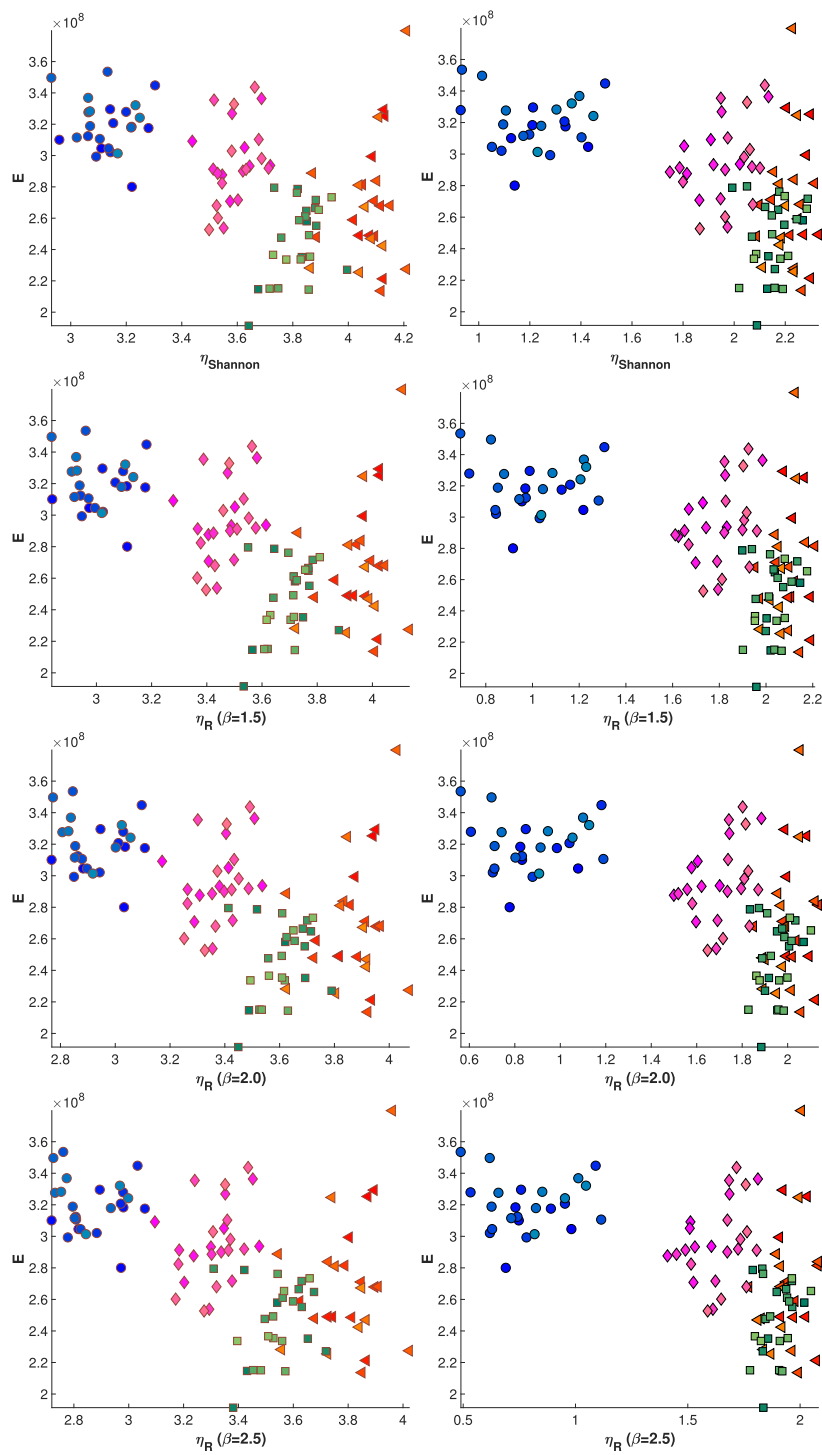


Figure 6. Young's modulus versus entropy. From top to bottom: Shannon, Rényi with $\beta = 1.5, 2.0, 2.5$ respectively. (Left) for the size statistics, (right) for the number of sides statistics.

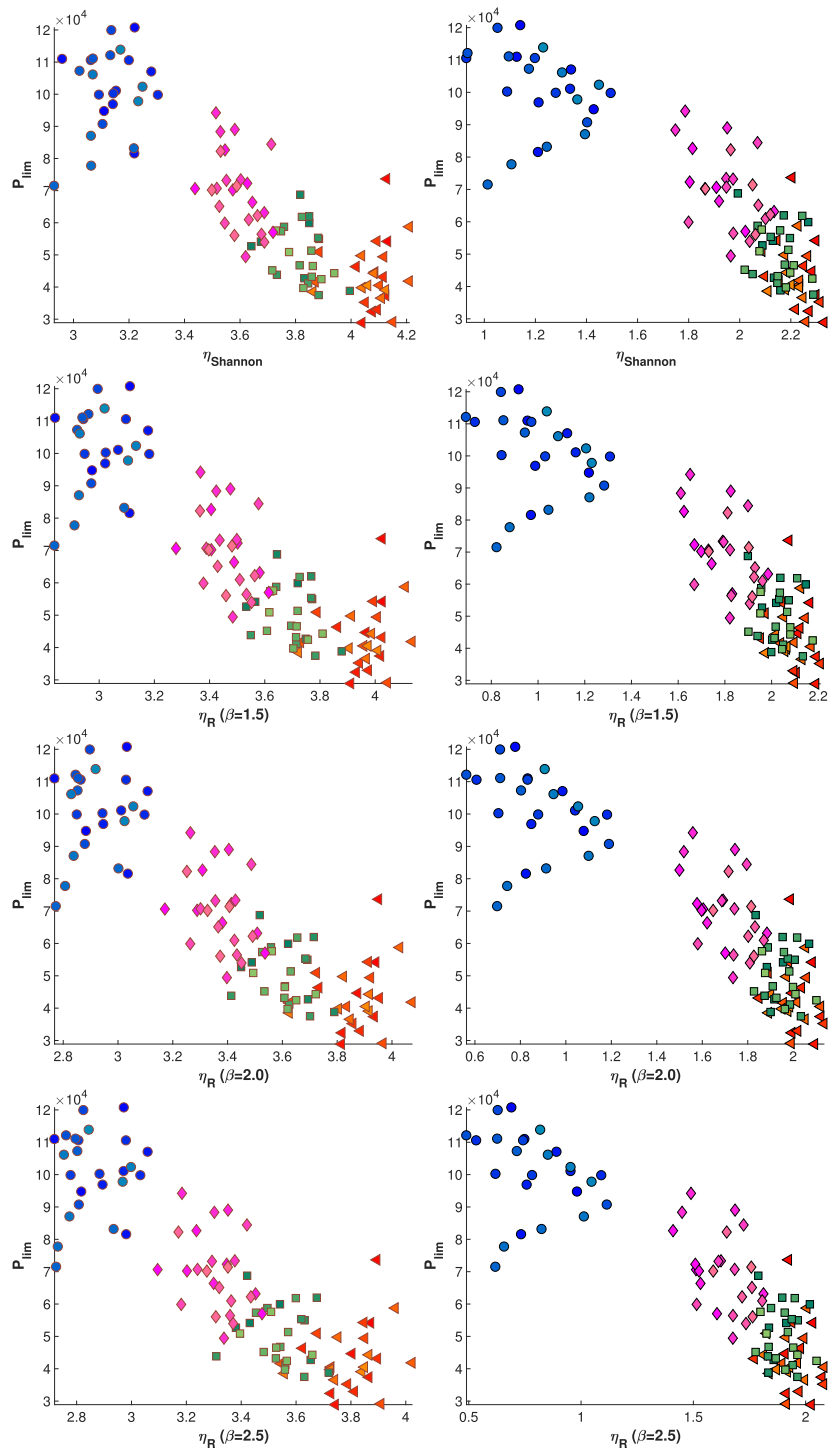


Figure 7. Proportional limit versus entropy. From top to bottom: Shannon, Rényi with $\beta = 1.5, 2.0, 2.5$ respectively. (Left) for the size statistics, (right) for the number of sides statistics.

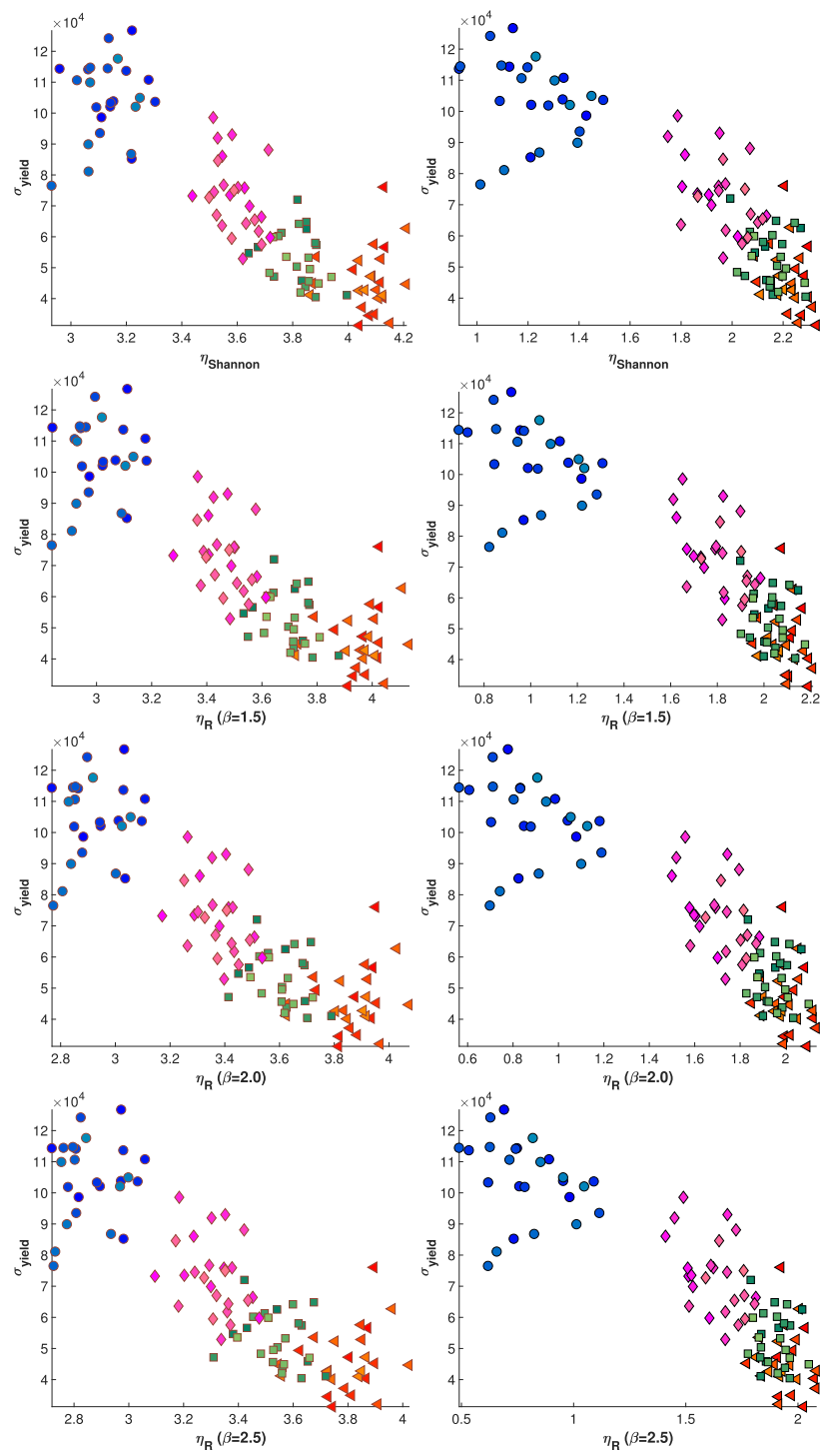


Figure 8. First yield stress versus entropy. From top to bottom: Shannon, Rényi with $\beta = 1.5, 2.0, 2.5$ respectively. (Left) for the size statistics, (right) for the number of sides statistics.

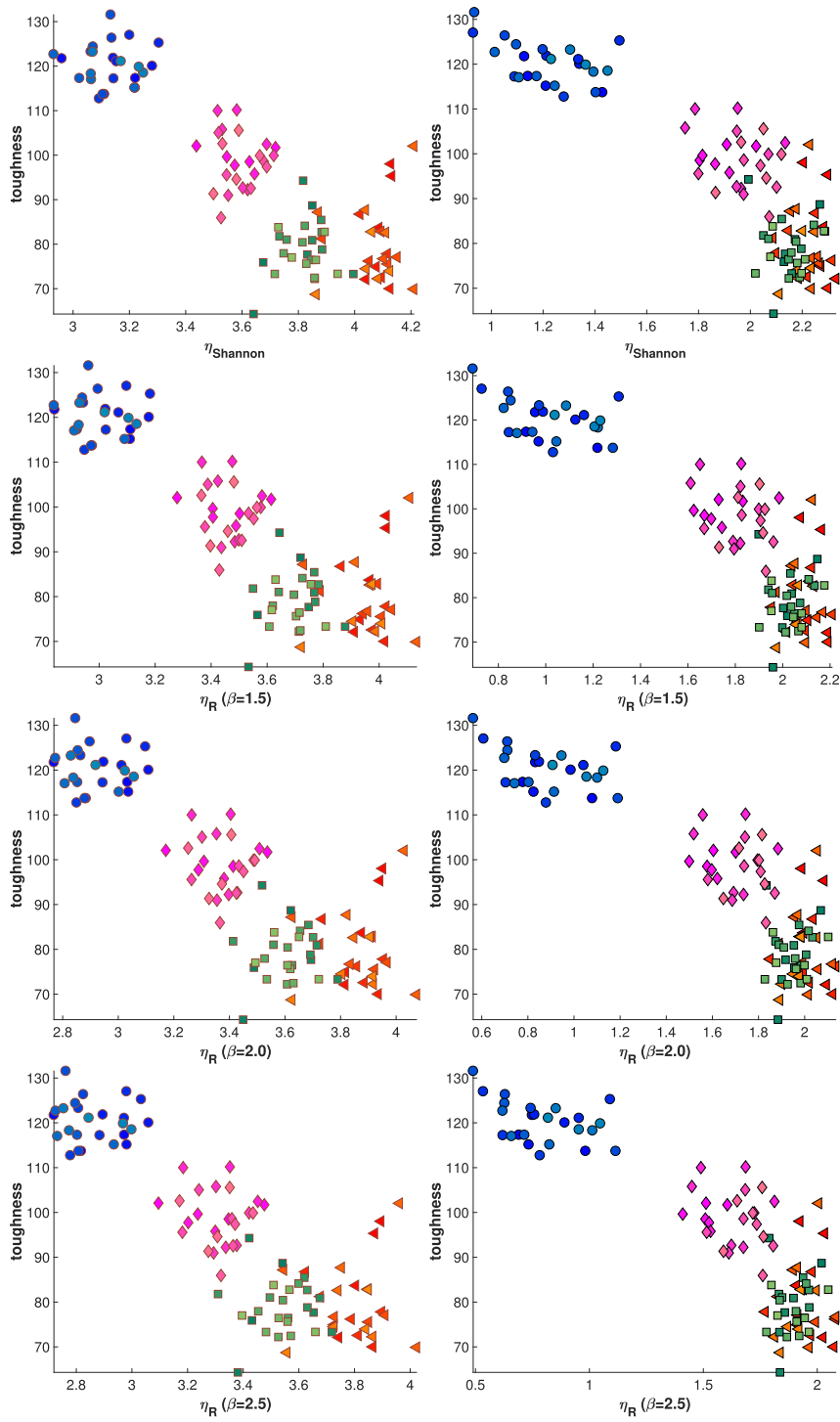


Figure 9. Toughness versus entropy. From top to bottom: Shannon, Rényi with $\beta = 1.5, 2.0, 2.5$ respectively. (Left) for the size statistics, (right) for the number of sides statistics.

size based entropy. This clustering is based on the perturbation type used to construct the Voronoi cells (representative of grains), thus there are four visible clusters, one for each reference microstructure. All the above suggests that, not only the type of entropy used to reveal dependence of the mechanical parameters on the topological information is important, but also the features considered to calculate those entropy values, such as size and side distributions.

Another important insight from these scatter plots is that they could provide meaningful information when attempting to design materials with specific mechanical properties. For example, if the goal is to design a material with toughness values ranging between $100 \text{ Pa} \times \%$ and $110 \text{ Pa} \times \%$, the plots suggest that the material should have a Shannon size-based entropy value ranging between 3.4379 and 3.7188 and the type of microstructure best suitable to get this desired feature could be Weibull-Voronoi.

In addition to looking at entropy calculations, *distances* from the hexagonal microstructure based on Jensen divergence concept were calculated using equations (5) and (6) for the limiting case $\beta \rightarrow 1$. The elastic parameters were also plotted against their corresponding distance values: Young's modulus in figure 10, proportional limit in figure 11, first yield stress in figure 12 and toughness in figure 13.

From these plots, it is worth noting that for the size based distance calculations the Rényi–Jensen divergence based distance definition with parameter $\beta = 2.5$ is the one which shows the clearest dependence between the mechanical parameters and the distance values, the other types of distances are less conclusive since data is more spreadout. Similarly, as in the entropy plots, this dependence has a nonlinear decreasing trend in which the Normal-Voronoi microstructure type appears as the closest in distance to the hexagonal microstructure; which is expected since this type is the one with more six-side grains than the rest of the other types of microstructures. On the other hand, for the side based distance calculations, it is the Jensen–Shannon divergence based distance the one that shows the clearest dependence.

A sensitivity analysis of the elastic response versus entropy values based on the number of grains was also performed. We ran uniaxial compression simulations on 5 samples for each microstructure type, each sample with different number of grains ranging from 200 grains up to 1700 grains. Samples were generated by varying the hexagonal lattice spacing and keeping constant the height to width ratio of the specimen. Results of this convergence analysis with areas-based and side-based entropy values are shown in figures 14 and 15 respectively. Left columns corresponds to samples with 350 and right columns corresponds to samples with 1020 grains. From top to bottom Young's modulus, proportional limit, first yield and toughness values are plotted against 11 different Rényi entropy values corresponding to variations of the β parameter from the limiting case (the Shannon entropy) up to 2.5. Results for Hexagonal, Normal-Voronoi, Lognormal-Voronoi, Poisson-Voronoi and Weibull-Voronoi microstructures are depicted with a star, circles, triangles, squares and diamonds respectively. We observed the hexagonal microstructures have the largest mechanical parameter values, the mechanical performance dependence on entropy values again shows a nonlinear decreasing trend as the number of grains is increased. We also noticed that as the number of grain increases, the Lognormal-Voronoi microstructures become marginally mechanically stronger than the Poisson-Voronoi and Weibull-Voronoi microstructure types. However, as a general trend we observed that the larger the entropy value the weaker the mechanical performance of the material no matter the number of grains in the specimen.

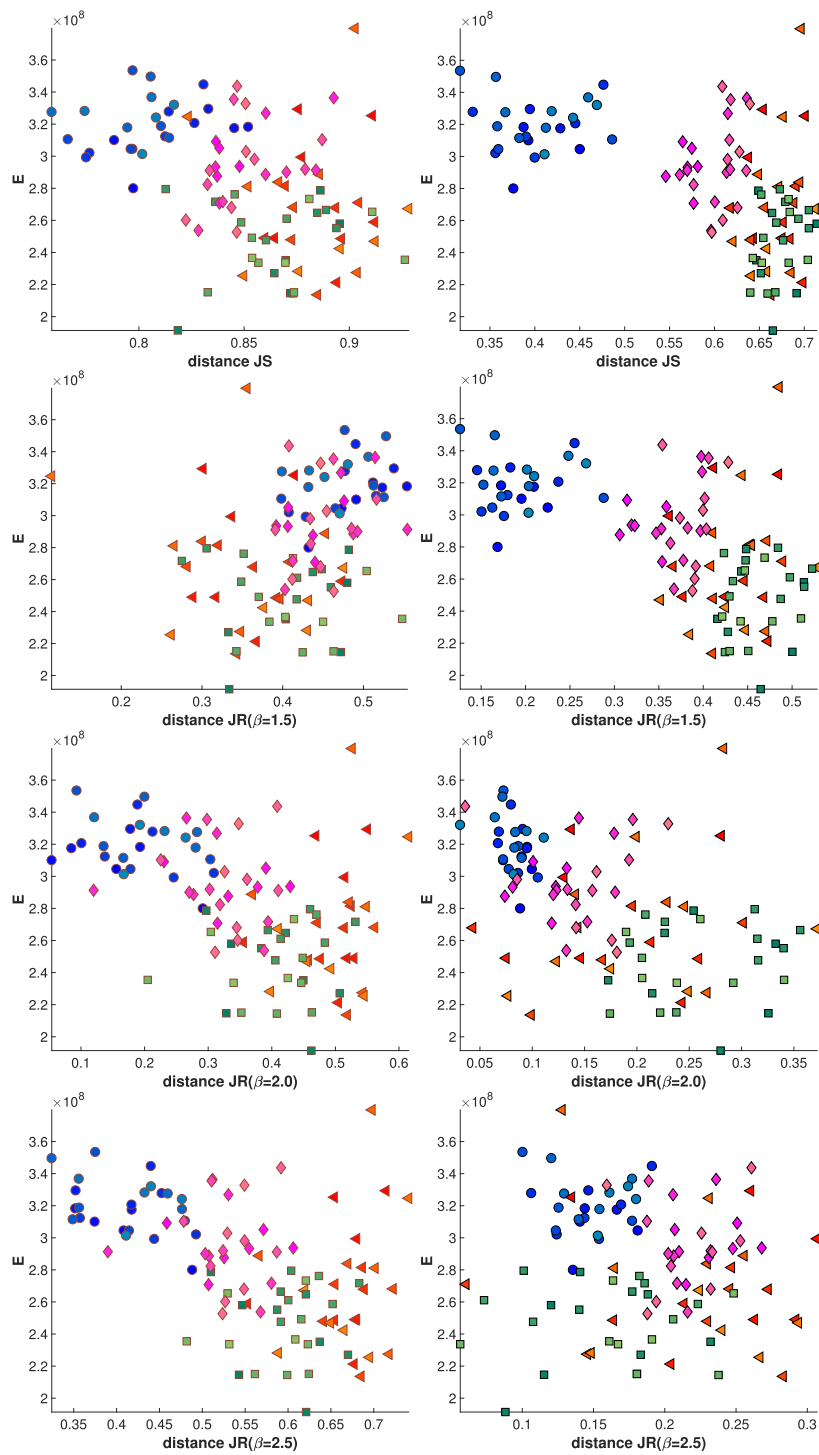


Figure 10. Young's modulus versus Jensen divergence based distance. From top to bottom: Shannon, Rényi with $\beta = 1.5, 2.0, 2.5$ respectively. (Left) for the size statistics, (right) for the number of sides statistics.

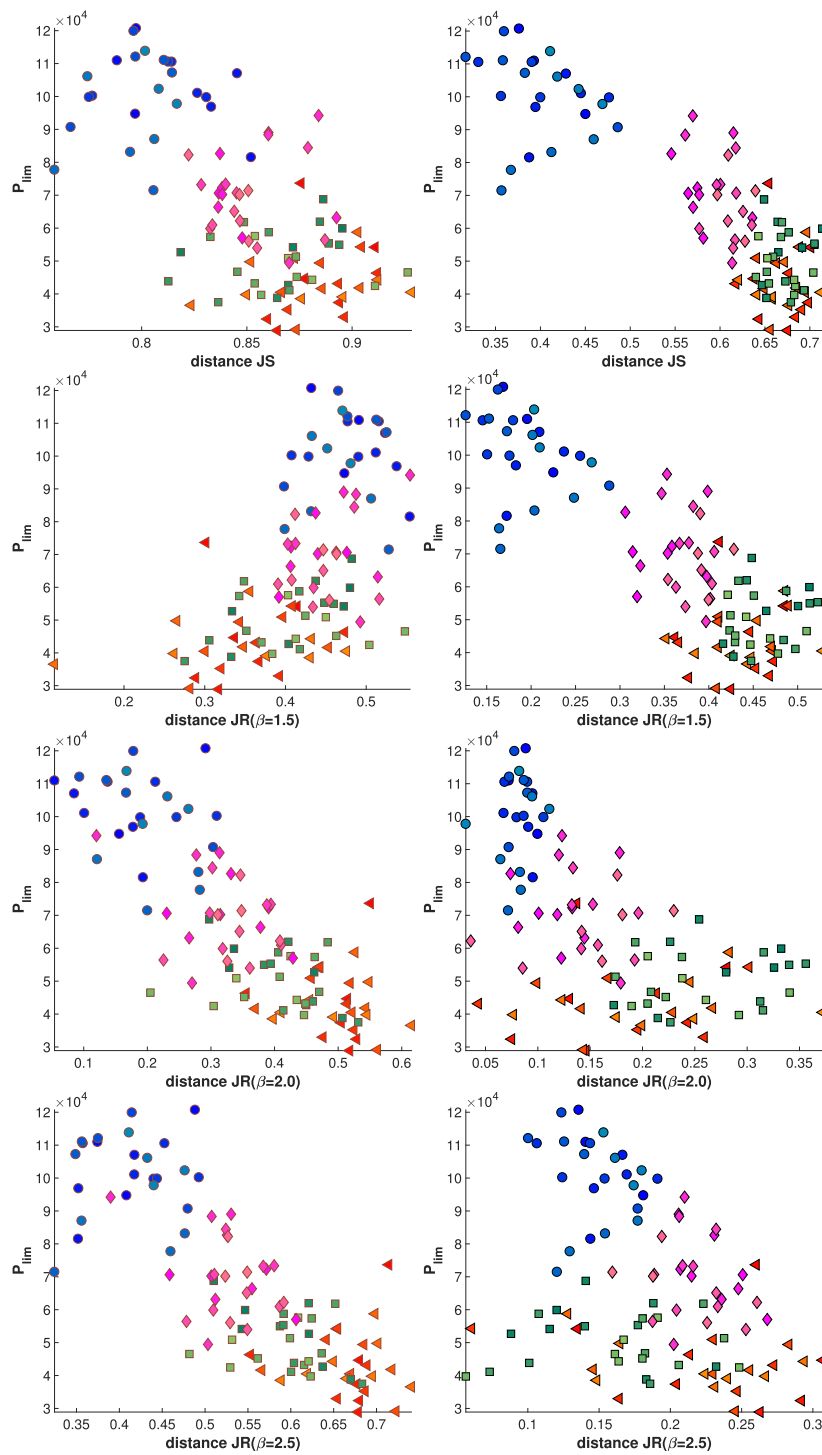


Figure 11. Proportional limit versus Jensen divergence based distance. From top to bottom: Shannon, Rényi with $\beta = 1.5, 2.0, 2.5$ respectively. (Left) for the size statistics, (right) for the number of sides statistics.

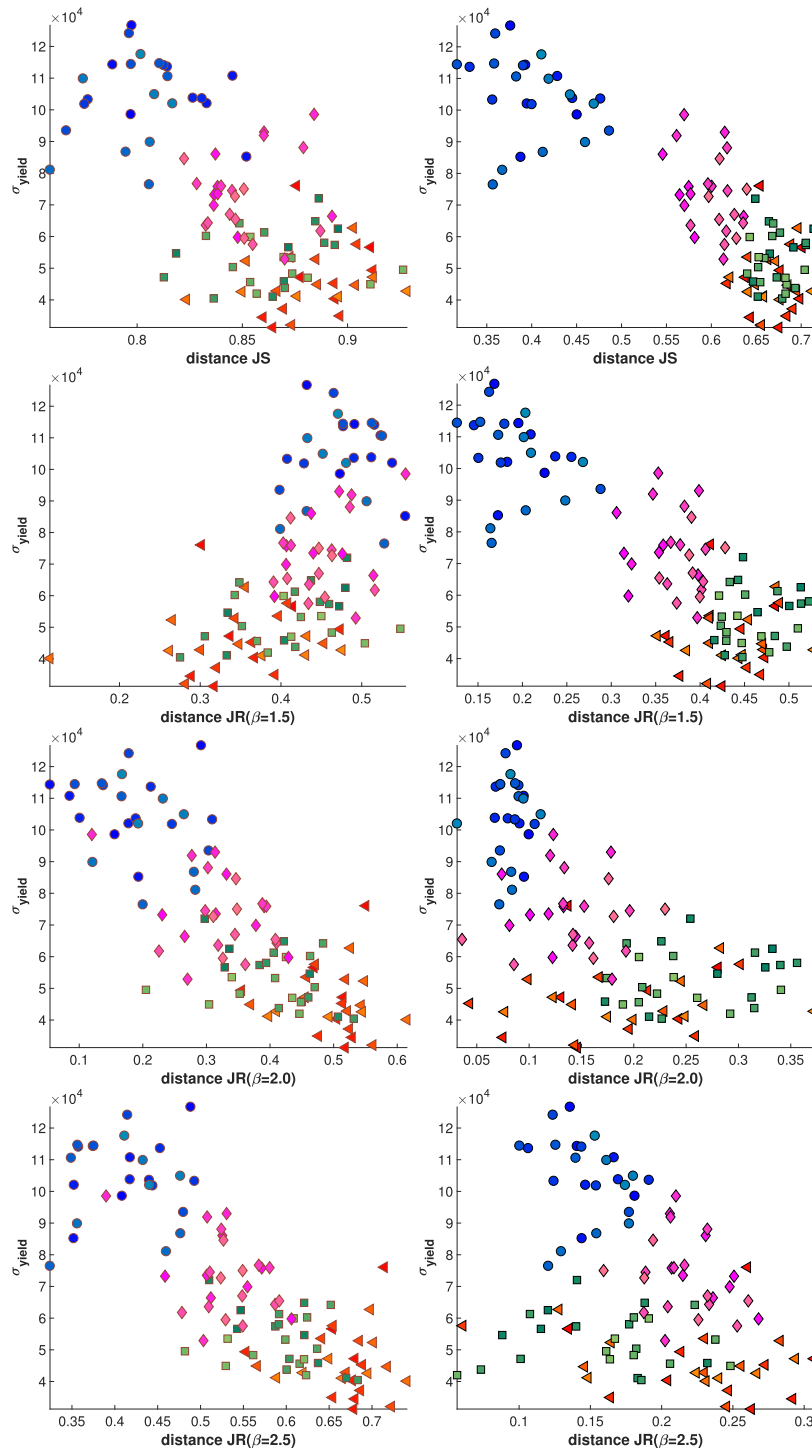


Figure 12. First yield stress versus Jensen divergence based distance. From top to bottom: Shannon, Rényi with $\beta = 1.5, 2.0, 2.5$ respectively. (Left) for the size statistics, (right) for the number of sides statistics.

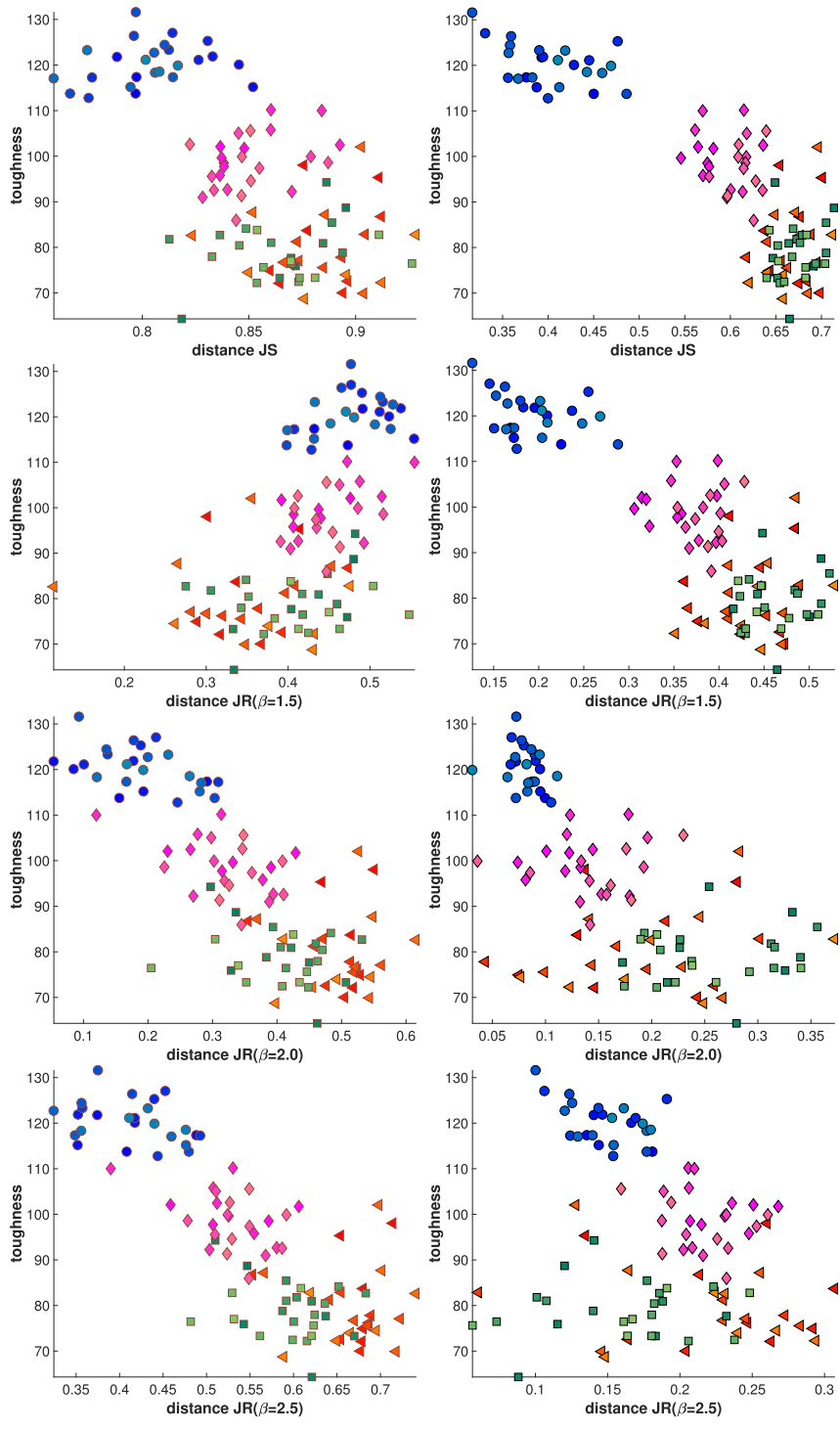


Figure 13. Toughness versus Jensen divergence based distance. From top to bottom: Shannon, Rényi with $\beta = 1.5, 2.0, 2.5$ respectively. (Left) for the size statistics, (right) for the number of sides statistics.

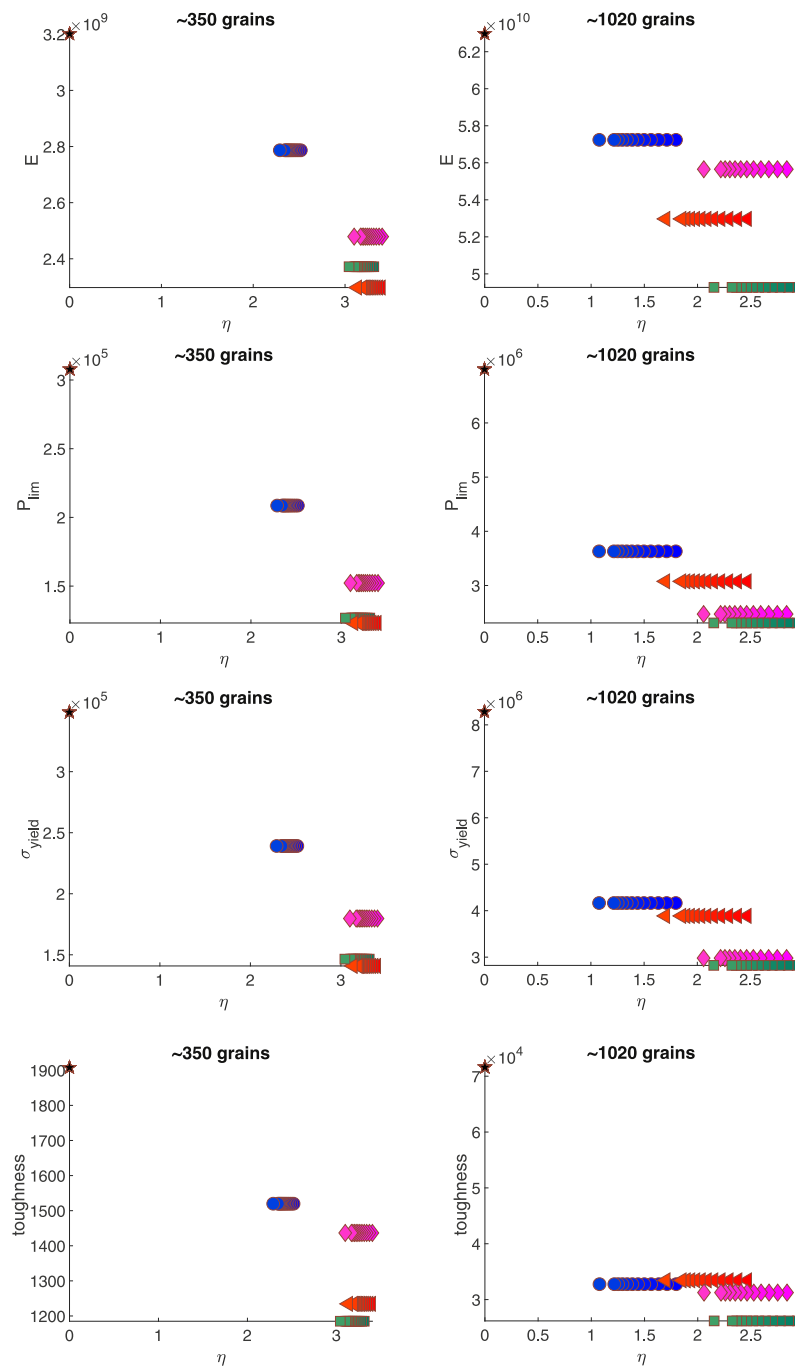


Figure 14. Sensitivity analysis of the elastic response versus areas-based entropy values based on the number of grains: (left) 350 grains and (right) 1020 grains. Hexagonal (star), Normal-Voronoi (circles), Lognormal-Voronoi (triangles), Poisson-Voronoi (squares) and Weibull-Voronoi (diamonds).

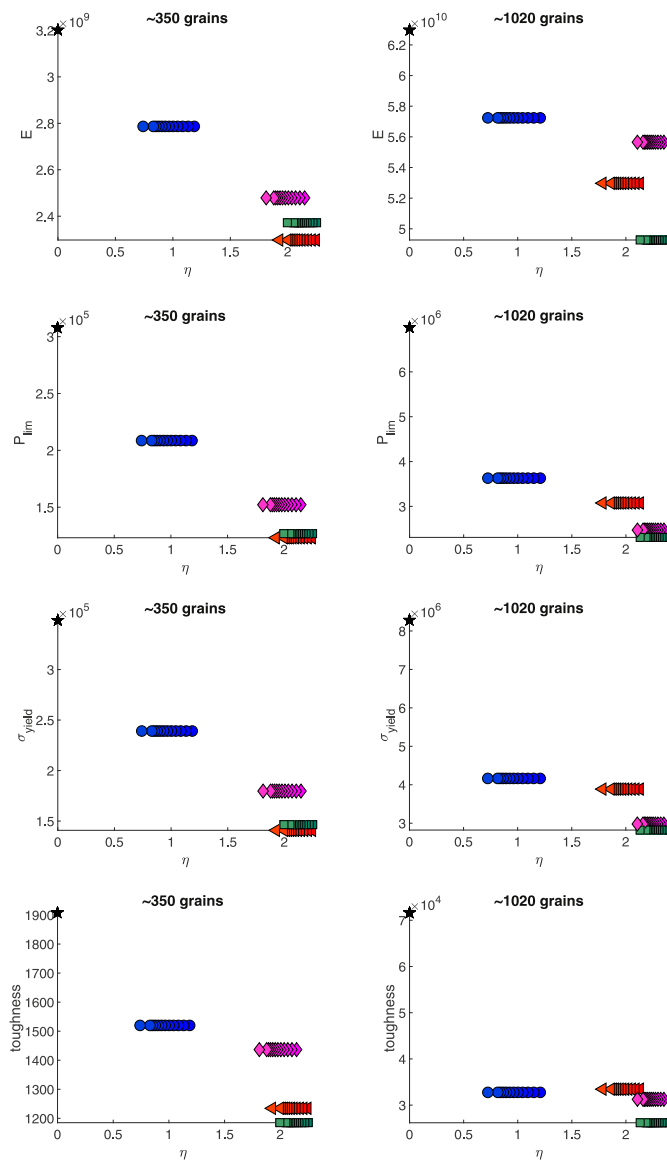


Figure 15. Sensitivity analysis of the elastic response versus side-based entropy values based on the number of grains: (left) 350 grains and (right) 1020 grains. Hexagonal (star), Normal-Voronoi (circles), Lognormal-Voronoi (triangles), Poisson-Voronoi (squares) and Weibull-Voronoi (diamonds).

3.3. Damage response

Finally, the dependence of the microstructure damage, in terms of grain boundary failure, on the microstructure topology and geometry was also explored. Figure 16 shows the bonded contact network at the first and last time step of the DEM simulation for the microstructure with highest first yield stress within each set and the hexagonal microstructure. Bonded contacts are depicted as darker points and non-bonded contacts as lighter points. From

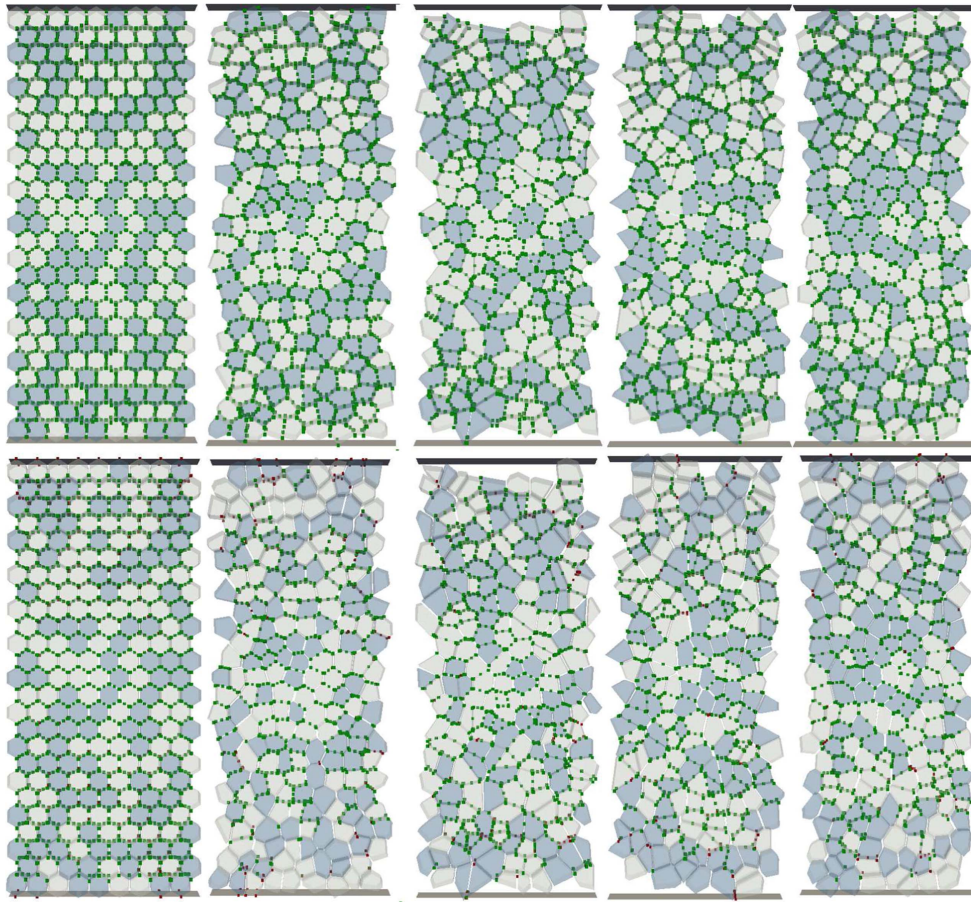


Figure 16. Bonded contact network at the first (top row) and last (bottom row) time steps. From left to right: Hexagonal, Normal-Voronoi, Weibull-Voronoi, Poisson-Voronoi and Lognormal-Voronoi microstructures.

figure 16 it is observed that there is less damage within the specimen with hexagonal microstructure than the rest of microstructures. This is quantified with the ratio $C_r = \frac{\text{Contacts}_{|t=t_0}}{\text{Contacts}_{|t=t_f}}$, the ratio of the number of bonded contacts at time t_0 versus the number of bonded contacts at the end of the simulation denoted as t_f . The smaller C_r the larger the number of bonded contacts remaining and therefore the microstructure presents less damage. Table 4 shows the mean and median of bonded contacts ratios for each microstructure set. This ratio is the smallest for the hexagonal microstructure compared with the others, $C_r^{\text{hex}} = 1.6725$. Table 5 shows the corresponding mean and median of Shannon and Rényi ($\beta = 1.5$) entropy values for each microstructure set, for both size and side distributions. It can be seen that as the entropy increases the mean and median of the ratios C_r decrease, with the exception of the hexagonal case which has zero entropy and the smallest contact ratio C_r ; or in other words, the larger the amount of topological and geometrical disorder in the grain boundary network facilitates resistance to crack propagation. In fact, the Lognormal microstructure has the largest mean and median entropy values while having the largest number of bonded contacts remaining at t_f , or second smallest contact ratio $C_r^{\text{Log}} = 2.4131$. Hence, these

Table 4. Mean and median of bonded contacts for each set of microstructures.

Type	C_r	
	Mean	Median
Normal	3.3201	3.3101
Weibull	2.7884	2.7954
Poisson	2.6325	2.6063
Lognormal	2.4069	2.4131

Table 5. Shannon and Rényi ($\beta = 1.5$) entropy values for each microstructure set.

Type	Size distribution				Side distribution			
	η_S		η_R		η_S		η_R	
	Mean	Median	Mean	Median	Mean	Median	Mean	Median
Normal	3.1346	3.1371	3.0102	2.9955	1.2228	1.2134	1.0150	0.9889
Weibull	3.5915	3.5812	3.4639	3.4755	1.9562	1.9646	1.8031	1.8212
Poisson	3.8196	3.8322	3.6960	3.7144	2.1517	2.1581	2.0270	2.0325
Lognormal	4.0728	4.0931	3.9571	3.9741	2.2200	2.2338	2.0902	2.0960

Table 6. Jensen–Shannon and Rényi–Jensen ($\beta = 1.5$) divergence based distance values for each microstructure set.

Type	Size distribution				Side distribution			
	Dist _{JS}		Dist _{JR}		Dist _{JS}		Dist _{JR}	
	Mean	Median	Mean	Median	Mean	Median	Mean	Median
Normal	0.8040	0.8057	0.4770	0.4772	0.4029	0.3947	0.1948	0.1831
Weibull	0.8505	0.8465	0.4500	0.4469	0.5997	0.6087	0.3718	0.3776
Poisson	0.8672	0.8697	0.4107	0.4172	0.6722	0.6689	0.4609	0.4483
Lognormal	0.8834	0.8849	0.3526	0.3557	0.6675	0.6715	0.4342	0.4436

entropy-based metrics do not seem to reflect the trend that we see in the amount of damage observed by DEM.

To better elucidate this dependence, we looked at the distance metric in addition to the entropy metric. Table 6 shows the corresponding mean and median of Jensen–Shannon and Jensen–Rényi ($\beta = 1.5$) divergence based distance values for each microstructure set, for both size and side distributions. When using size-based and side-based Jensen–Shannon distance and side-based Jensen–Rényi distance, a similar trend as the entropy trend is observed: as the distance increases the ratio C_r decreases. This suggests that these three distance metrics are not well suitable to reflect the amount of damage observed by DEM either. However, when using size-based Jensen–Rényi ($\beta = 1.5$) distance metric, depicted in bold columns table 6, we can clearly observe the decrease in C_r values when the distance from hexagonal microstructure decreases. In this particular case, the Lognormal microstructure is the closest to the hexagonal microstructure both in terms of mean ($\text{Dist}_{JR,\beta=1.5} = 0.3526$) and median ($\text{Dist}_{JR,\beta=1.5} = 0.3557$) distance values and in terms of the number of bonded contacts. This phenomenon confirms the importance of investigating

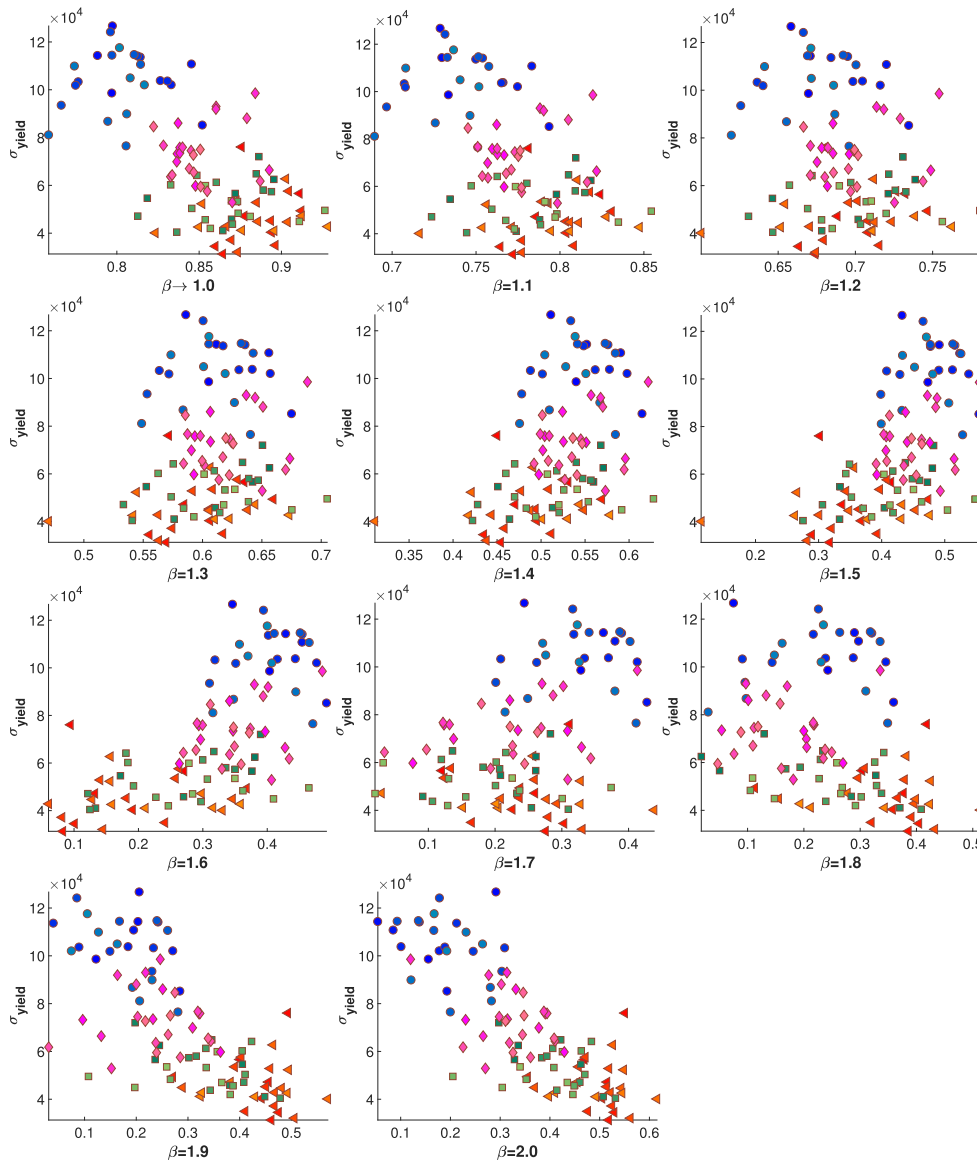


Figure 17. Size-based Jensen–Rényi distance metrics with β varying from the limiting case 1.0 through 2.0.

the topology-performance response and geometrical-performance response of 2D polycrystalline materials in terms not only of one specific entropy metric but several of them and also in terms of different distance metrics.

The fact that the relationship between the mechanical parameters and the size-based Jensen–Rényi ($\beta = 1.5$) distance metric showed a trend completely opposite to the other three distance metrics (Shannon and $\beta = 2.0, 2.5$), encouraged us to investigate further distance metrics with β varying from the limiting case 1.0 through 2.0. Figure 17 shows the trend for each case. For β values between the limiting case 1.0 and 1.2 we observed a decreasing trend,

then a switch to a increasing trend for $1.2 < \beta \leq 1.7$ and again a switch to a decreasing trend for $1.7 < \beta \leq 2.0$.

4. Summary and conclusions

In this work, we used relatively simple topological and geometrical measures to analyze the sensitivity of the mechanical response, as quantified by a DEM simulation, to the microstructure topology. Five types of microstructure were generated and for each one of them Rényi entropies with parameter $\beta = 1.5, 2.0, 2.5$ and the limiting case $\beta \rightarrow 1$ (corresponding to the Shannon entropy) were calculated as an approach for characterizing 2D polycrystalline materials topology, based on the grain sizes and grain number of sides distributions.

Simulations of quasi-static uniaxial compression loading tests over rectangular specimens were performed by using a grain-level micro-mechanical DEM to reveal dependence of materials mechanical properties on the mesoscale topological information. 25 rectangular specimens were generated for each reference microstructure set: Normal-Voronoi, Weibull-Voronoi, Poisson-Voronoi and Lognormal-Voronoi. The grains were assumed to be made of an idealized material with properties described in tables 1 and 2.

Overall, results revealed that the larger the entropy values the weaker the mechanical performance of the material measured by Young's modulus, proportional limit, first yield stress and toughness in DEM simulations. These observations are especially important when choosing appropriate initial configuration for various large-scale simulations.

Also, for each microstructure type, their corresponding mechanical parameters have their own range of values; suggesting that this approach could potentially be beneficial when attempting to design materials with specific mechanical response.


By looking at different entropy and distance metrics it was also observed that different metrics should be taken into account when trying to expose dependence of different mechanical properties on the mesoscale topological and geometrical information. Namely, different types of features can be extracted from different metrics. This study suggests that Shannon entropy could be the best candidate metric for designing materials with certain Young's modulus, proportional limit, first yield stress and toughness. However, size-based Rényi distance metrics might work better when it comes to quantifying bond breakage.

Acknowledgments

This research was supported by National Science Foundation grant DMS-1056821. The authors are extremely grateful to the anonymous referees for carefully going over the manuscript and offering valuable suggestions that helped us improve that quality of the presentation. The authors are also grateful to John F Peters, Mississippi State University, for the fruitful discussions and valuable suggestions to improve this work. The *ERDC-DEM* code used in this work was initially developed at the Engineer Research and Development Center (ERDC). The computational experiments were run on ARGO, a research computing cluster provided by the Office of Research Computing at George Mason University, VA. (<http://orc.gmu.edu>).

ORCID iDs

Katerine Saleme Ruiz  <https://orcid.org/0000-0003-3411-7541>

Maria Emelianenko  <https://orcid.org/0000-0002-3209-4705>

References

- [1] Mason K K, Lazar E A, MacPherson R D and Srolovitz D J 2012 *Phys. Rev. E* **86** 051128
- [2] D’Addetta G A and Ramm E 2006 *Gran. Matter* **8** 159–74
- [3] Hoshide T 2011 *JMEPEG ASM Int.* **20** 1497–504
- [4] Yildis Y O and Kirca M 2017 *Model. Simul. Mater. Sci. Eng.* **25** 025008
- [5] Srolovitz D J, Grest G S, Anderson M P and Rollett A D 1988 *Acta Metall.* **36** 2115–28
- [6] Rollett A D, Srolovitz D J, Doherty R D and Anderson M P 1989 *Acta Metall.* **37** 627–39
- [7] Lee S-B, Rohrer G S and Rollet A D 2014 *Model. Simul. Mater. Sci. Eng.* **22** 025017
- [8] A-iyeh E S and Peters J 2016 *Theory Appl. Math. Comput. Sci.* **6** 77–95
- [9] Wakai F, Enomoto N and Ogawa H 2000 *Acta Mater.* **48** 1297–311
- [10] Krill C III and Chen L-Q 2002 *Acta Mater.* **50** 3059–75
- [11] Resk H, Delannay L, Bernacki M, Coupez T and Logé R 2009 *Model. Simul. Mater. Sci. Eng.* **17** 075012
- [12] Brahme A, Alvi M, Saylor D, Fridy J and Rollett A 2006 *Scr. Mater.* **55** 75–80
- [13] Quey R, Dawson P R and Barbe F 2011 *Comput. Methods Appl. Eng.* **200** 1729–45
- [14] Silva M J, Hayes W C and Gibson L J 1995 *Int. J. Mech. Sci.* **37** 1161–77
- [15] Berdichevsky V L 2005 *J. Mech. Phys. Solids* **53** 2457–69
- [16] Berdichevsky V L 2008 *J. Mech. Phys. Solids* **56** 742–71
- [17] Nguyen T T, Réthoré J, Yvonnet J and Baietto M-C 2017 *Comput. Mech.* **60** 289–314
- [18] Sukumar N, Srolovitz D J, Baker J T and Prévost J 2003 *Int. J. Numer. Methods Eng.* **56** 2015–37
- [19] Psakhie S G *et al* 2001 *Theor. Appl. Fract. Mech.* **37** 311–34
- [20] Beese S, Loehnert S and Wriggers P 2016 Modeling of fracture in polycrystalline materials *Advances in Discretization Methods (SEMA SIMAI Springer Series vol 12)* (Cham: Springer) (https://doi.org/10.1007/978-3-319-41246-7_4)
- [21] Hallberg H 2013 *Modelling Simul. Mater. Sci. Eng.* **21** 085012
- [22] Rényi A 1961 *Proc. 4th Berkeley Symp. on Math. Statist. and Prob.* vol 1 (Berkeley, CA: University of California Press) pp 547–61
- [23] Horner D A, Peters J F and Carrillo A 1979 *ASCE J. Eng. Mech.* **127** 1027–32
- [24] Walizer L and Peters J F 2011 *J. Comput. Phys. Commun.* **182** 281–8
- [25] Potyondy D O and Cundall P A 2004 *Int. J. Rock Mech. Min. Sci.* **41** 1329–64
- [26] Hill R 1972 *Proc. R. Soc. A* **326** 131–47
- [27] Suquet P M 1985 Local and global aspects in the mathematical theory of plasticity *Plasticity Today: Modeling, Methods and Applications* ed A Sawceuk and G Bianchi (London: Elsevier) pp 279–310
- [28] Zhou M 2003 *Proc. R. Soc. A* **459** 2347–92
- [29] André D, Jebahi M, Iordanoff I, Charles J-L and Néauport J 2013 *Comput. Methods Appl. Mech. Eng.* **265** 136–47
- [30] Peters J F 2005 *J. Eng. Math.* **52** 231–50